UPCommons

Portal del coneixement obert de la UPC

http://upcommons.upc.edu/e-prints

Real-Time Wireless, Contactless and Coreless Monitoring of the Current Distribution in Substation Conductors for Fault Diagnosis

A. Kadechkar, J.-R. Riba, *Member, IEEE*, M. Moreno-Eguilaz, J. Sanllehí

Abstract—**Parallel conductors are found in electrical transmission and distribution systems including large ampacity feeders or loads. However, current unbalance often occurs, especially in alternating current systems. This non-regular current distribution causes overheating and premature ageing, facilitating the occurrence of failures. Therefore, a fault diagnosis system is a must, which can be performed by monitoring in real-time the individual currents flowing through the conductors. In this paper a setup including three parallel aluminum conductors of large cross section, a spacer and two terminal substation connectors is analyzed. A real-time, wireless, coreless and contactless system based on three low cost Hall effect sensors is proposed, which is also easy to install. Experimental results, which include fourteen cases, comprising thirteen fault modes and a well installed set, prove the suitability and potential of the proposed approach, since it allows a correct real-time detection of all analyzed faulty conditions as well as the detection of currents exceeding the thermal rating of the conductors.**

Index Terms—**Current distribution, blind source separation, non-intrusive current measurement, Hall effect, predictive maintenance, real-time monitoring, fault diagnosis.**

I. INTRODUCTION

NOWADAYS wireless sensor networks are being developed worldwide [1]–[4]. They can be applied for real time monitoring of different parameters in existing power grids, to enable them to be more controllable and reliable. Among the measured parameters, electric current plays a key role. It has been proved that this approach allows improving drastically power system reliability and availability [5] by determining the health condition of vital elements. By this way, early failure symptoms can be diagnosed, so that suitable measures to anticipate further degradation can be applied [6].

Electrical current sensors are widely used to measure electrical current in many applications, including alternating current (AC) and direct current (DC) applications, electrical power distribution and consumption systems, power electronics or residential applications among others [7]–[11]. Most of the solutions found in the technical literature are based on sensing the magnetic flux density. Sensors for large currents typically include a ferromagnetic core [6] for increasing the magnetic flux density and protecting the sensor from external magnetic influences [12]. Different authors have shown that in case of parallel conductors, by discretizing the Ampere's law [5], [12]–[15], it is possible to avoid the use of a ferromagnetic core, which is a bulky and costly solution [16], thus simplifying installation, reducing cost, reducing vibrations, avoiding nonlinearities due to saturation effects or minimizing corona effects in high-voltage applications. Due to the continuous improvements, multiple Hall effect sensors can be used simultaneously for blind source separation, that is, to recover the individual components of the current or magnetic flux density of different sources [17]. In [15] four Hall sensors were installed nearby four parallel conductors to determine their DC currents in the range below 100 A. Although other current sensors such as Rogowski coils or shunt resistors can be applied to measure large currents in parallel conductors, they usually modify the impedance of the conductors [15]. When reconstructing the currents from the readings of the sensors, the effects of external magnetic fields can have a significant influence [12]. Therefore, it is mandatory to find a suitable location to install the sensors in order to increase the distance between the interference source and the arrangement

Power connectors are key elements in transmission systems since they allow provide a continuous electrical path between electrical conductors or bus bars [18], [19]. Therefore, they are key elements of substations, playing a critical role in their reliability and efficiency, since failed connectors can cause major affectations in the entire substation [20], thus leading to catastrophic consequences and huge economic costs. These effects can be considerably reduced by continuously monitoring the state of the connector in order to predict the failure in advance, by applying a predictive maintenance plan.

Although electrical conductors supplied by DC present a homogeneous current density distribution, under AC supply it

A. Kadechkar is with the Universitat Politècnica de Catalunya, Electrical Engineering Department, Rambla Sant Nebridi 22, 08222 Terrassa, Spain (e-mail: akash.kadechkar@upc.edu) and also with SBI Connectors España, C. Albert Einstein, 5 - 7. Polígono Industrial Sesrovires, 08635 Sant Esteve de Sesrovires, Spain (e-mail: akash.kashinath@sbiconnect.es)

J.-R. Riba is with the Universitat Politècnica de Catalunya, Electrical Engineering Department, Rambla Sant Nebridi 22, 08222 Terrassa, Spain (e-mail: riba@ee.upc.edu)

M. Moreno-Eguilaz is with the Universitat Politècnica de Catalunya, Electronic Engineering Department, Rambla Sant Nebridi 22, 08222 Terrassa, Spain (e-mail: manuel.moreno.eguilaz@upc.edu)

J. Sanllehí is with SBI Connectors España, C. Albert Einstein, 5 - 7. Polígono Industrial Sesrovires, 08635 Sant Esteve de Sesrovires, Spain (e-mail: josep.sanllehi@sbiconnect.es)

tends to be not homogeneous due to the effects of the eddy currents [21], [22]. When analyzing multi-conductor systems such as the geometry analyzed in this work, eddy current phenomenon, which arise in the form of skin and proximity effects can be important [23], especially for conductors of large radiuses which are very close each other. It results in an increase of the effective AC resistance, thus raising power losses and the operating temperature of the conductors. Such effects, which cannot be ignored, limit the current carrying capacity of the conductors. Therefore, the AC resistance must be known, since it is a key design parameter [24]. However, it is not easy to calculate by means of analytical expressions, since even for the simplest configurations, such expressions are either very complex or are not available [22]. This problem can be solved by means of numerical methods [25]. Among them, the finite element method (FEM) highlights, due to its flexibility and accurate results.

This paper analyzes the current distribution in three large conductors of the same phase, which are connected in parallel and share the total phase current. The conductors carrying very large currents ($\approx$ 1000 A) are joined by the means of two terminal substation connectors. It estimates the current in each conductor by sensing the magnetic flux density around all conductors [8], using non-intrusive coreless and contactless Hall effect sensors [16]. In the technical literature there are very few works analyzing the behavior of such sensors for very large current applications [12], [14]. This paper proposes to apply a predictive maintenance strategy by continuously monitoring the current in the three parallel and identical conductors of the same phase used in an AC substation, which are usually separated by means of aluminum spacers. Even using spacers, the proximity effect, which produces inductance differences [15], remains important, thus leading to an uneven current distribution among the three conductors. A real case is analyzed, in which, once installed, it was detected an uneven current distribution among the three parallel conductors due to the proximity effect and poor installation practices, that finally led to a major failure. This uneven current distribution is aggravated by the fact that the contact resistances between the conductors and the terminal connectors are different, which can be intensified due to poor installation practices and ageing, thus unbalancing even more the three currents, the associated power losses and the temperatures of the individual connectors. In this paper it is shown that the contact resistance between the terminal connectors and the conductors is critical to determine the amount of current passing through each conductor. This uneven current distribution produces different thermal stresses in the conductors, and thus, one of the conductor ages faster than the others. This situation can eventually lead to premature and sudden failure, which can cause catastrophic consequences in the substation.

To minimize the effects of the analyzed problem, this paper proposes applying a predictive maintenance plan based on monitoring the currents of the three conductors in real-time. By this way the amount of current in any conductor and the current unbalance among the conductors can be monitored. To ensure a safe operation of the system, the current in each conductor must be less than its ampacity, that is, the maximum constant current that the conductor can safely carry to meet security, safety and design criteria under defined thermal conditions [26], [27]. This work proposes to use three coreless Hall Effect sensors to measure in real-time the electrical currents through the three conductors. This solution allows minimizing the number of Hall effect sensors while reducing maintenance requirements and the uncertainty due to interfering nearby sources of magnetic flux density generated by external current carrying elements [8]. This approach also allows performing a real-time diagnosis and quantify the current distribution unevenness, while ensuring that the three conductors operate below their thermal ratings.

II. HALL EFFECT SENSORS FOR LARGE CURRENT SENSING

The current flowing through a conductor can be measured with different type of sensor technologies, including current transformers, Rogowski coils, shunt resistors, or analog-bipolar Hall effect sensors [28], [29] among others. However, when focusing on high-current applications in the range 100-3000 A, and taking into account several features such as sensor accuracy, size, cost, low weight or maintenance requirements among others, the Hall effect sensor is an appropriate choice [30]. In the case of low-current applications, this sensor is often combined with a toroidal magnetic core, thus being unsuitable for the application studied in this paper [30], [31], due to the dimensions of the toroidal magnetic core that facilitates corona appearance conditions in high-voltage applications, the generated vibrations, the added extra weight and cost and the difficulty to assemble. These disadvantages can be overcome by using coreless Hall effect sensors, due to the high magnetic flux density close to the conductors.

The Hall effect sensor generates an output voltage which is related to the magnitude of the magnetic flux density. Since the magnetic flux density near a conductor is proportional to the current carrying this conductor, the output voltage can be related to the current. This type of sensor allows performing a contactless measurement of both DC and AC electrical currents, this being another advantage of this technology.

The relationship between the output voltage provided by the sensor V_{Hall} and the external magnetic flux density B [T] due to the conductor can be written as follows [15], [30],

$$B = \frac{V_{Hall}}{k \cdot [1 + k_T \cdot (t - 25)]} = \frac{V_{Hall}}{K(t)} \qquad (1)$$

where k [V/T] is the sensitivity of the Hall effect sensor, k_T [0.0012 ºC^{-1}] is the sensitivity correction factor due to temperature, and t [ºC] the actual temperature of the sensor.

It is worth noting that the sensitivity k is affected by positioning tolerances [31], conductor dimensions or orientation of the sensor. To minimize the error, it must be calibrated, if possible, *in situ* by means of a reference Rogowski coil.

From (1), it results,

$$k = \frac{V_{Hall}}{B \cdot [1 + k_T \cdot (t - 25)]} \qquad (2)$$

As explained, coreless Hall effect sensors are selected for this application, considering that they are placed in a known and fixed position, and that the radius r of the conductor and the distance h are also known. Under this assumption, when dealing with a single rectilinear conductor of circular cross-section, according to the Biot–Savart law [30] and Fig. 1 it results,

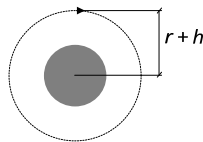$$B = \frac{\mu_0 I}{2\pi(r+h)} \qquad (3)$$

Fig. 1. Magnetic flux line generated by a rectilinear conductor of radius r at a distance h from its surface.

According to (3), since $\mu_o = 4\pi \cdot 10^{-7}$ [N/A^2], if the magnetic flux density and B the position $r + h$ [m] of the sensor are known, the current I [A] in the conductor can be obtained as,

$$I = \frac{B \cdot (r+h)}{2 \cdot 10^{-7}} \qquad (4)$$

III. WIRELESS COMMUNICATIONS

The system proposed in this work is compatible with wireless communications. It features a low-cost, small-size and very low power consumption solution. Fig. 2 shows the sensors and wireless communication system based on the Bluetooth SoC nRF52832 from Nordic Semiconductors. The Bluetooth system transmits the data to a gateway, which is further processed by means of Matlab®, which applies the equations detailed in Sections II and IV.

The gateway used in this work is a standard PC (Intel® Core™ i7-3770 CPU 3.4 GHz) with Bluetooth compatibility, although many other solutions are possible, depending on the specific application [32], [33].
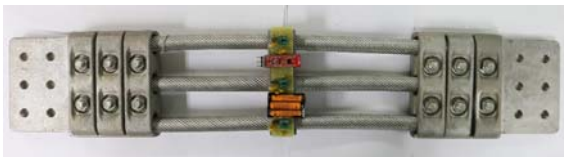
Fig. 2. The analyzed connectors, spacer and conductors with the sensors and the wireless communication system.

IV. MATHEMATICAL MODEL

This section sets the mathematical equations that describe the relationship between the currents and the magnetic flux density strength close to the three parallel conductors shown in Fig. 3. Therefore, the equations for blind source separation are detailed.

In the arrangement shown in Fig. 3a, due to the three parallel conductors of the same phase, there is an asymmetrical flux density distribution due to the effects of any conductor on the remaining ones (see Fig. 3b). This, in turn, produces an uneven distribution of the current density in each conductor, and thus, the outer conductors tend to carry more current than the central one. In practical cases, this effect can be boosted because of the different contact resistances between the individual conductors

and the connector, and the different contact pressure of the conductors. It is noted that there are only two bolts for the three conductors in every cap, as shown in Fig. 2.
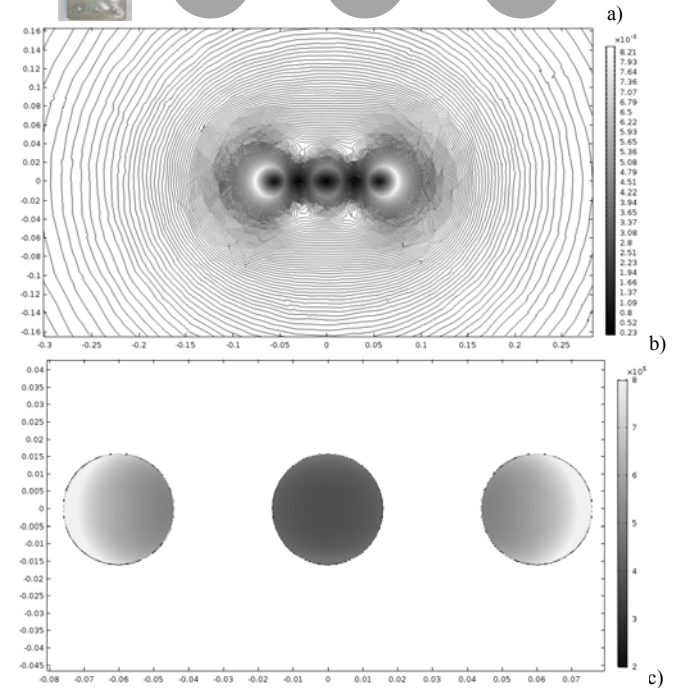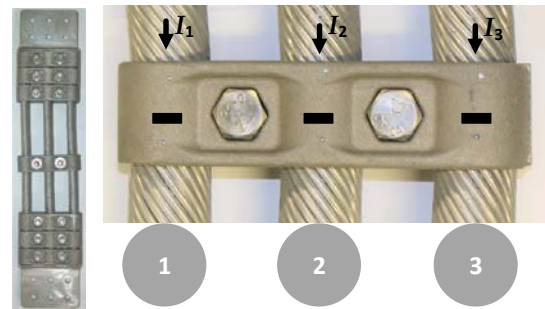
Fig. 3. a) Analyzed connectors, spacer and conductors. There are three parallel aluminum conductors of circular cross-section connected to the same phase. The black rectangles correspond to the Hall effect sensors mounted close to the conductors. b) Magnetic flux density contour plot (T) obtained from FEM simulations. c) Uneven current density (A/m^2) in the three conductors due to the effects of eddy currents obtained from FEM simulations.

A. Determination of the three currents from the magnetic field close to the conductors

The magnetic flux density seen by any of the three Hall sensors displayed in Fig. 4a is affected by the magnetic flux densities generated by the two adjacent conductors.
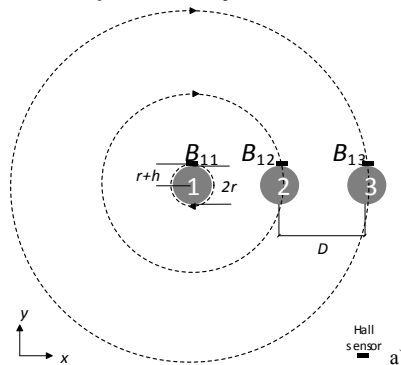
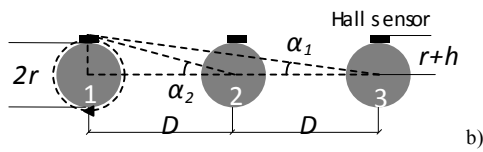Fig. 4. a) Three-conductors forming a go circuit. Magnetic flux density distribution generated by conductor 1. Note that B_{12} is the magnetic flux density generated by conductor 1 affecting Hall sensor 2. b) Detail of the angles α_1 and α_2 used to determine the components of the magnetic flux density.

Assuming different currents in the three conductors I_1, I_2 and I_3, respectively, the x and y components of the magnetic flux density seen by the three Hall sensors can be calculated as follows.

$$\begin{cases} B_{11x} = \dfrac{\mu_0 \cdot I_1}{2 \cdot \pi \cdot (r+h)} \\[2mm] B_{11y} = 0 \\[2mm] B_{21x} = \dfrac{\mu_0 \cdot I_2}{2 \cdot \pi \cdot \sqrt{D^2 + (r+h)^2}} \cdot \sin(\alpha_2) \\[2mm] B_{21y} = \dfrac{\mu_0 \cdot I_2}{2 \cdot \pi \cdot \sqrt{D^2 + (r+h)^2}} \cdot \cos(\alpha_2) \\[2mm] B_{31x} = \dfrac{\mu_0 \cdot I_3}{2 \cdot \pi \cdot \sqrt{D^2 + (r+h)^2}} \cdot \sin(\alpha_1) \\[2mm] B_{31y} = \dfrac{\mu_0 \cdot I_3}{2 \cdot \pi \cdot \sqrt{D^2 + (r+h)^2}} \cdot \cos(\alpha_1) \end{cases} \quad (5)$$

The modulus of the magnetic flux density seen by the Hall sensor placed in conductor 1, B_1, is calculated as,

$$B_1 = \sqrt{(B_{11x} + B_{21x} + B_{31x})^2 + (B_{11y} + B_{21y} + B_{31y})^2} \quad (6)$$

The angle α_1 between the center of the external conductor and the opposite external sensor, and α_2 between the center of the middle conductor and the external sensor (Fig. 4b) are given as,

$$\begin{cases} \alpha_1 = \operatorname{atan}\left(\dfrac{r+h}{2 \cdot D}\right) \\[3mm] \alpha_2 = \operatorname{atan}\left(\dfrac{r+h}{D}\right) \end{cases} \quad (7)$$

Similarly, the modulus of the magnetic flux density seen by the Hall sensor placed near conductor 2 (B_2), can be calculated as,

$$\begin{cases} B_{12x} = \dfrac{\mu_0 \cdot I_1}{2 \cdot \pi \cdot \sqrt{D^2 + (r+h)^2}} \cdot \sin(\alpha_2) \\[2mm] B_{12y} = -\dfrac{\mu_0 \cdot I_1}{2 \cdot \pi \cdot \sqrt{D^2 + (r+h)^2}} \cdot \cos(\alpha_2) \\[2mm] B_{22x} = \dfrac{\mu_0 \cdot I_2}{2 \cdot \pi \cdot (r+h)} \\[2mm] B_{22y} = 0 \\[2mm] B_{32x} = \dfrac{\mu_0 \cdot I_3}{2 \cdot \pi \cdot \sqrt{D^2 + (r+h)^2}} \cdot \sin(\alpha_2) \\[2mm] B_{32y} = \dfrac{\mu_0 \cdot I_3}{2 \cdot \pi \cdot \sqrt{D^2 + (r+h)^2}} \cdot \cos(\alpha_2) \end{cases} \quad (8)$$

The modulus of the magnetic flux density seen by the Hall sensor placed in the central conductor, B_2, can be calculated as,

$$B_2 = \sqrt{(B_{12x} + B_{22x} + B_{32x})^2 + (B_{12y} + B_{22y} + B_{32y})^2} \quad (9)$$

Finally, B_3, the modulus of the magnetic flux density seen by the Hall sensor placed near conductor 3, can be calculated as,

$$\begin{cases} B_{13x} = \dfrac{\mu_0 \cdot I_1}{2 \cdot \pi \cdot \sqrt{D^2 + (r+h)^2}} \cdot \sin(\alpha_1) \\[2mm] B_{13y} = -\dfrac{\mu_0 \cdot I_1}{2 \cdot \pi \cdot \sqrt{D^2 + (r+h)^2}} \cdot \cos(\alpha_1) \\[2mm] B_{23x} = \dfrac{\mu_0 \cdot I_2}{2 \cdot \pi \cdot \sqrt{D^2 + (r+h)^2}} \cdot \sin(\alpha_2) \\[2mm] B_{23y} = -\dfrac{\mu_0 \cdot I_2}{2 \cdot \pi \cdot \sqrt{D^2 + (r+h)^2}} \cdot \cos(\alpha_2) \\[2mm] B_{33x} = \dfrac{\mu_0 \cdot I_3}{2 \cdot \pi \cdot (r+h)} \\[2mm] B_{33y} = 0 \end{cases} \quad (10)$$

$$B_3 = \sqrt{(B_{13x} + B_{23x} + B_{33x})^2 + (B_{13y} + B_{23y} + B_{33y})^2} \quad (11)$$

B. Mathematical model for single-axis Hall effect sensors

The sensors used in this work are only sensitive to one axis, for instance the x axis. The mathematical development provided in (5) - (11) takes into account both x and y components of the magnetic flux density. Therefore, when only considering the x component of the magnetic flux density, (6), (9) and (11) can be rewritten as,

$$B_1 = \sqrt{(B_{11x} + B_{21x} + B_{31x})^2} \quad (12)$$

$$B_2 = \sqrt{(B_{12x} + B_{22x} + B_{32x})^2} \quad (13)$$

$$B_3 = \sqrt{(B_{13x} + B_{23x} + B_{33x})^2} \quad (14)$$

C. Initial calibration of the Hall sensor sensitivity

To calibrate the three Hall effect sensors, their sensitivity must be estimated. The calibration can be done experimentally by comparing their output values with those provided by a calibrated Rogowski coil. The readings of the Rogowski coil, that is, I_{1ref}, I_{2ref} and I_{3ref} can be substituted into (5), (8) and (10), thus obtaining the resulting magnetic flux densities B_1, B_2 and B_3 from (12), (13) and (14), respectively.

Next, from B_1, B_2 and B_3, once the voltage provided by each individual sensor is known, and by applying (2), the sensitivity of each sensor is obtained.

D. After-calibration stage

Once the Hall sensors are calibrated, they can measure their respective magnetic flux densities. By applying (5), (8) and (10) and substituting into (12), (13) and (14), respectively, a three equation system emerges, in which the unknown variables are I_1, I_2 and I_3. Next, by using the *vpa* solver from Matlab® or a similar alternative, the three currents through the conductors I_1, I_2 and I_3 can be obtained.

The procedure to calibrate the sensors and to determine the three individual I_1, I_2 and I_3 from the readings of the three Hall sensors is summarized in Fig. 5.
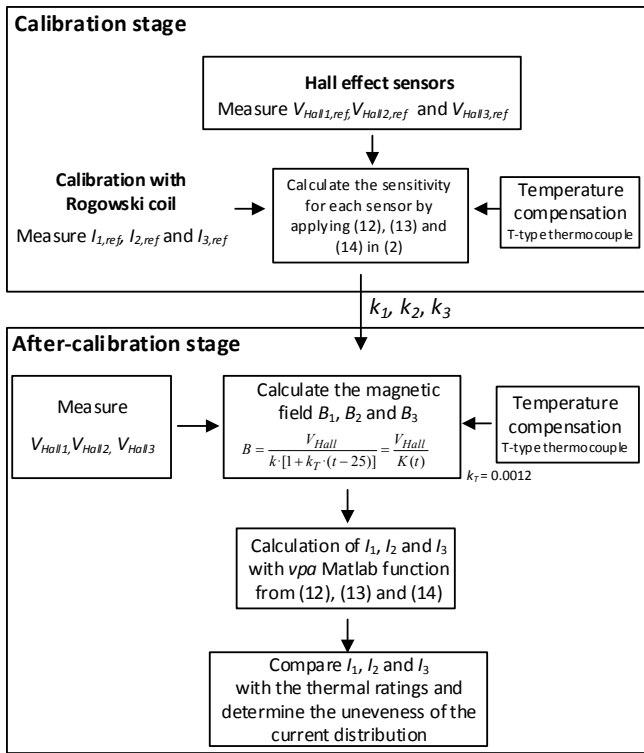
Fig. 5. Flowchart of the blind source approach presented in this paper for determining the three currents I_1, I_2 and I_3 under AC power frequency supply.

V. CONTACT RESISTANCE OF THE THREE CONDUCTORS

In this section the resistances between the three conductors and the connector are calculated to prove that even with a suitable installation, these different resistances aggravate the uneven current distribution among the three conductors.

Fig. 6 shows the procedure applied to measure the resistances between the three conductors and the connector.

When determining the three resistances between the conductors and the terminal connector according to the procedure shown in Fig. 6, the following equation arises,

$$I_{1,i} + I_{2,i} + I_{3,i} = I_{Total,i}$$
$$\frac{\Delta V_{1,i}}{R_1} + \frac{\Delta V_{2,i}}{R_2} + \frac{\Delta V_{3,i}}{R_3} = I_{Total,i} \tag{15}$$

Since in (15) there are three unknowns (R_1, R_2 and R_3), to determine the values of the unknowns, three equations are required ($i = 1, 2, 3$). This issue was solved by applying three external current levels (50, 100 and 200 A_{DC}) to measure $I_{Total,i}$ and $\Delta V_{1,i}$, $\Delta V_{2,i}$ and $\Delta V_{3,i}$ with $i = 1, 2, 3$. This method allows quantifying the resistance unbalance among the three conductors, so it can be useful during installation. Finally, the three equations in (15) can be solved simultaneously to obtain the individual resistances R_1, R_2 and R_3.
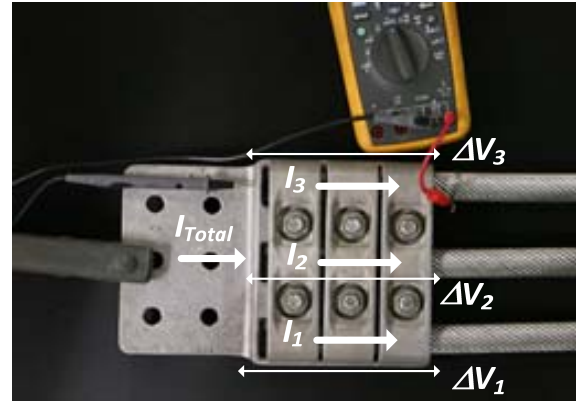

Fig. 6. Measurement of the contact resistance by using a Centurion micro-ohmmeter from Raytech. The total current I_{Total} was measured with the micro-ohmmeter, whereas the voltage drops ΔV_1, ΔV_2 and ΔV_3 were measured with a Fluke 289 digital multimeter.

Table 1 shows the resistance values obtained by applying this method. Such values clearly indicate an unbalance of the individual resistances, and hence, an unbalance of the currents flowing through each conductor, even when applying good installation practices.

Table 1. Individual resistances between the conductors and the connector in both connectors calculated by applying (15)

Connector 1			Connector 2		
Resistance ($\mu\Omega$)			Resistance ($\mu\Omega$)		
R_1	R_2	R_3	R_1	R_2	R_3
9.7	10.0	4.8	9.8	6.5	10.0

The unbalance in the resistances is due to several factors including small imperfections in the inner contact surfaces between the conductor and the connector or differ contact pressures of the three conductors, since they are not symmetrically bolted, among others. The effect of the uneven resistances adds up to the effect of the uneven current distribution due to the proximity effect, as shown in Fig. 3c, such effects being unavoidable. They can be aggravated due to poor installation practices, non-parallel installation of the conductors, or the effects of nearby elements carrying current such as conductors, bus bars or return paths among others. Thus, the best option is to minimize the contact resistance as much as possible. To this end it is necessary to brush the inner surface of the connector and the outer surfaces of the conductors and to apply grease in the interfaces between the conductors and the connector, as well as to ensure an adequate torque in all bolting elements.

VI. EXPERIMENTAL RESULTS

This section summarizes the experimental results performed to validate the correct behavior of the proposed system. The elements used during the experiments are displayed in Fig. 7.

Fig. 7. a) Experimental setup used in this work including the conducting loop with the three conductors, the spacer and the terminal connectors, the high-current transformer and the three Hall sensors. b) Terminal connectors, spacer and the three conductors.

As shown in Fig. 7, the test loop is composed of bus bars of rectangular cross section, which are connected to the two terminal connectors, the spacer and three aluminum conductors (length = 1 m and diameter = 32 cm) with an ampacity of 1015 A. Three DRV5053 analog-bipolar Hall effect sensors from Texas Instruments and a 4000D Rogowski coil from Chauvin Arnoux were used to measure the current in the conductors. A T-type thermocouple connected to a Fluke 51 II digital thermometer was used to measure the temperature.

A. Comparison of the results of the proposed system against those of the Rogowski coil

In this section the results provided by the approach proposed in this paper based on the three Hall sensors and developed in Section IV, are compared against the values provided by a calibrated Rogowski coil. They are summarized in Table 2.

Table 2. Comparative results between the measurements performed with the calibrated Rogowski coil and the proposed system

Total (A)	Rogowski coil (A)			Proposed system (A)			Error (%)		
I_{Total}	I_1	I_2	I_3	I_1	I_2	I_3	I_1	I_2	I_3
≈ 300	110	86	105	107	89	97	2.6	3.3	7.5
≈ 650	243	192	234	245	193	227	0.7	0.6	3.0
≈ 1000	368	290	351	363	297	350	1.2	2.6	0.4
≈ 1350	495	389	472	491	404	471	0.7	3.8	0.3
≈ 1600	592	466	564	589	473	590	0.5	1.5	4.7
≈ 1950	710	560	679	702	575	687	1.1	2.6	1.1
≈ 2250	830	655	791	822	691	795	0.9	5.5	0.5
≈ 2550	928	736	886	937	748	899	0.9	1.6	1.5
≈ 2900	1052	835	999	1065	852	1025	1.2	2.0	2.6
≈ 3200	1171	934	1113	1206	907	1154	3.0	2.9	3.7

Results summarized in Table 2 clearly show a good agreement between the measurements performed with the calibrated Rogowski coil and those performed with the proposed method.

B. Current mismatch for induced faults

In this section several experiments were performed to force different faults. This strategy was applied in order to verify whether the proposed system is able to detect these different faults. To this end, 14 scenarios are analyzed, which are summarized in Fig. 8.
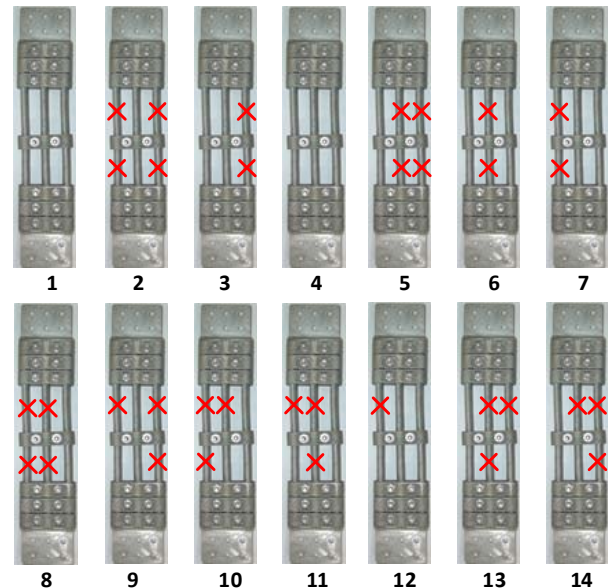

Fig. 8. The fourteen analyzed scenarios. The red crosses represent a total disconnection of the section of the conductor.

The 14 cases summarized in Fig. 8 were analyzed under five operating conditions each. Therefore, a total of 70 (14x5) experiments were conducted. The five operating conditions correspond to different current levels through the conductors. It is noted that case 1 corresponds to a well installed connector, whereas the remaining ones correspond to fault cases. In addition, case 4 presents a resistance mismatch because an asymmetry in the input and output bus bars.

Figs. 9 show the current measured by the Rogowski coil through the three conductors and those measured by the three Hall effect sensors after applying the mathematical processing according to (5) - (14).

Experimental results presented in Fig. 9 show a good match between the results attained with the approach proposed in this paper and those provided by the Rogowski coil. Main differences can be due to the fact that Hall sensors have some sensitivity in the y axis (although much less than in the x axis), and also due to geometrical differences of the experimental setup from the three straight wires geometry, thus causing a distortion of the magnetic flux density which is not considered in Section IV. It is worth noting that in this application, accuracy requirements of the proposed system are quite low, since it only has to check that the three currents are below a certain threshold value given by the thermal rating of the conductors or by a current mismatch among the conductors.
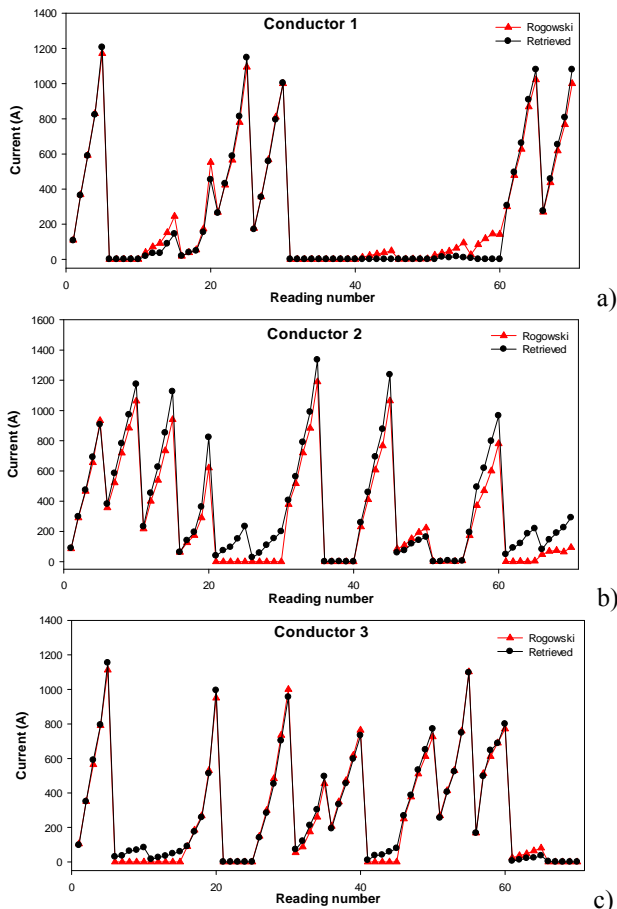
Fig. 9. Comparative results between the method proposed in this work and the ones provided by the Rogowski coil. a) Current through conductor 1. b) Current through conductor 2 (central conductor). c) Current through conductor 3.

C. Fault condition detection

Table 3 shows the current distribution for the analyzed cases, including a well installed connector and 13 fault modes.

Table 3. Current distribution in each conductor in percentage with respect to the total current for the fourteen analyzed cases.

Case	Average current in % with respect to the total current			Fault induced	Fault detected
	I_1	I_2	I_3		
1	36.2	29.2	34.7	No fault	No fault
2	0.0	93.3	6.7	Cond. 1 and 3 disconnected	Yes
3	7.7	87.2	5.1	Cond. 3 disconnected and resistance mismatch	Yes
4	13.3	37.3	49.4	Resistance mismatch	Yes
5	85.2	14.8	0.0	Cond. 2 and 3 disconnected	Yes
6	49.2	8.9	41.9	Cond. 2 disconnected and resistance mismatch	Yes
7	0.0	79.1	20.9	Cond. 1 disconnected and resistance mismatch	Yes
8	0.0	0.1	99.9	Cond. 1 and 2 disconnected	Yes
9	0.0	94.2	5.8	Cond. 1 and 3 disconnected	Yes
10	0.0	17.5	82.5	Cond. 1 and 2 disconnected	Yes
11	1.6	0.5	97.9	Cond. 1 and 2 disconnected	Yes
12	0.3	52.0	47.7	Cond. 1 disconnected and resistance mismatch	Yes
13	82.5	15.3	2.2	Cond. 2 and 3 disconnected	Yes
14	77.4	22.4	0.2	Cond. 2 and 3 disconnected	Yes

From the results summarized in Table 3 it is concluded that fault conditions can be detected when any of the conductors carries less than 20% of the total current, this being the threshold value proposed in this work. Since by means of the proposed wireless real-time system the faults can be detected, an alarm signal can be generated in the event of a fault.

D. Thermal rating limitation

Another potential fault situation is when the current in any of the conductors exceeds its ampacity or thermal rating. Table 4 illustrates this problem when analyzing case 1, corresponding to a well installed connector. This potentially dangerous situation can be predicted by means of the real-time monitoring of the currents in each conductor, thus producing an alarm when the current through any of the conductors is higher than 100% of its ampacity.

Table 4. Case 1 corresponding to the three connected conductors. Current distribution in each conductor in percentage with respect to the ampacity

Case 1	% of maximum ampacity (1015 Amps)		
Total current (A)	Conductor 1 (%)	Conductor 2 (%)	Conductor 3 (%)
293.4	10.6	8.8	9.6
664.9	24.1	19.0	22.4
1010.6	35.8	29.3	34.5
1365.7	48.4	39.8	46.4
1652.3	58.0	46.6	58.2
1963.4	69.2	56.6	67.7
2308.2	81.0	68.1	78.3
2583.6	92.3	73.7	88.6
2941.8	104.9*	83.9	101.0*
3266.9	118.8*	89.4	113.7*

*Alarm triggered because the current is higher than the ampacity

VII. Conclusion

In this paper a non-intrusive coreless and contactless arrangement using three Hall effect sensors has been proposed for blind source separation of the three currents generated by three parallel substation conductors of the same phase. This system allows a simple, low cost and light weight solution for real-time monitoring with very low maintenance requirements. By analyzing fourteen cases including a well installed connector and thirteen fault modes, it has been shown that the proposed approach allows a correct real-time detection of 100% of the fault modes. Even more, the proposed system also allows detecting currents above the thermal rating of any conductor, thus preventing the whole arrangement from overheating and premature ageing. These good results justify the use of the proposed method for early fault detection in parallel conductors in real-time using coreless, small size and low cost sensors.

Acknowledgment

References

[1]   M. Ayaz, M. Ammad-Uddin, I. Baig, and E. H. M. Aggoune, "Wireless

sensor's civil applications, prototypes, and future integration possibilities: A review," *IEEE Sens. J.*, vol. 18, no. 1, pp. 4–30, 2018.

[2] E. U. Ogbodo, D. Dorrell, and A. M. Abu-Mahfouz, "Cognitive Radio Based Sensor Network in Smart Grid: Architectures, Applications and Communication Technologies," *IEEE Access*, vol. 5, pp. 19084–19098, 2017.

[3] M. Hajikhani, L. Fabrice, and B. L. Agba, "An Autonomous Wireless Sensor Network in a Substation Area Using Wireless Transfer of Energy," *IEEE Access*, vol. 6, pp. 62352–62360, 2018.

[4] H. Wu and M. Shahidehpour, "Applications of Wireless Sensor Networks for Area Coverage in Microgrids," *IEEE Trans. Smart Grid*, vol. 9, no. 3, pp. 1590–1598, 2018.

[5] Y. Xiang, K.-L. Chen, Q. Xu, Z. Jiang, and Z. Hong, "A Novel Contactless Current Sensor for HVDC Overhead Transmission Lines," *IEEE Sens. J.*, vol. 18, no. 11, pp. 4725–4732, Jun. 2018.

[6] Z. Li, Q. Li, Z. Wu, J. Yu, and R. Zheng, "A Fault Diagnosis Method for On Load Tap Changer of Aerospace Power Grid Based on the Current Detection," *IEEE Access*, vol. 6, pp. 24148–24156, 2018.

[7] C. Meetoo, S. Bahadoorsingh, N. Ramsamooj, and C. Sharma, "Wireless residential power monitoring system," *2017 IEEE Manchester PowerTech, Powertech 2017*, 2017.

[8] A. Bernieri, L. Ferrigno, M. Laracca, and A. Rasile, "An AMR-Based Three-Phase Current Sensor for Smart Grid Applications," *IEEE Sens. J.*, vol. 17, no. 23, pp. 7704–7712, Dec. 2017.

[9] S. Lee, Y. Ahn, T. Kim, N. Kim, and S. Lee, "A Superpositioning Technique for Accurate Open-Type Current Sensing in Three-Phase Electrical Switchboards," vol. 18, no. 22, pp. 9297–9304, 2018.

[10] J. Han, J. D. Jeong, I. Lee, and S. H. Kim, "Low-cost monitoring of photovoltaic systems at panel level in residential homes based on power line communication," *IEEE Trans. Consum. Electron.*, vol. 63, no. 4, pp. 435–441, 2017.

[11] G. Geng, J. Wang, K. L. Chen, and W. Xu, "Contactless Current Measurement for Enclosed Multiconductor Systems Based on Sensor Array," *IEEE Trans. Instrum. Meas.*, vol. 66, no. 10, pp. 2627–2637, 2017.

[12] A. Itzke, R. Weiss, T. DiLeo, and R. Weigel, "The Influence of Interference Sources on a Magnetic Field-Based Current Sensor for Multiconductor Measurement," *IEEE Sens. J.*, vol. 18, no. 16, pp. 6782–6787, Aug. 2018.

[13] G. D'Antona, L. Di Rienzo, R. Ottoboni, and A. Manara, "Processing magnetic sensor array data for AC current measurement in multiconductor systems," *IEEE Trans. Instrum. Meas.*, vol. 50, no. 5, pp. 1289–1295, 2001.

[14] A. Itzke, R. Weiss, and R. Weigel, "Influence of the Conductor Position on a Circular Array of Hall Sensors for Current Measurement," *IEEE Trans. Ind. Electron.*, vol. 66, no. 1, pp. 580–585, Jan. 2019.

[15] M. Park, S. Byun, W. Kim, J. Lee, K.Choi, and H. Lee, "Non-Contact Measurement of Current Distribution in Parallel Conductors by Using Hall Sensors," *IEEE Trans. Appl. Supercond.*, vol. 18, no. 2, pp. 1135–1138, Jun. 2008.

[16] N. George and S. Gopalakrishna, "Development of a New Low-Cost and Reliable Core-Less Current Probe for Conductor With Reduced Access," *IEEE Sens. J.*, vol. 17, no. 14, pp. 4619–4627, Jul. 2017.

[17] A. Paraschiv-Ionescu, C. Jutten, and G. Bouvier, "Source separation based processing for integrated Hall sensor arrays," *IEEE Sens. J.*, vol. 2, no. 6, pp. 663–673, Dec. 2002.

[18] F. Capelli, J.-R. J.-R. Riba, and J. Sanllehí, "Finite element analysis to predict temperature rise tests in high-capacity substation connectors," *IET Gener. Transm. Distrib.*, vol. 11, no. 9, pp. 2283–2291, Jun. 2017.

[19] ANSI/NEMA, "ANSI/NEMA CC1. Electric Power Connection for Substation." Rosslyn, Virginia, 2009.

[20] J. J.-A. Wang, J. Jy-An, J. K. Chan, and J. A. Graziano, "The Lifetime Estimate for ACSR Single-Stage Splice Connector Operating at Higher Temperatures," *IEEE Trans. Power Deliv.*, vol. 26, no. 3, pp. 1317–1325, Jul. 2011.

[21] J.-R. Riba, "Calculation of the ac to dc resistance ratio of conductive nonmagnetic straight conductors by applying FEM simulations," *Eur. J. Phys.*, vol. 36, no. July, pp. 1–10, 2015.

[22] V. T. Morgan, "The Current Distribution, Resistance and Internal Inductance of Linear Power System Conductors—A Review of Explicit Equations," *IEEE Trans. Power Deliv.*, vol. 28, no. 3, pp. 1252–1262, Jul. 2013.

[23] J.-R. Riba, "Analysis of formulas to calculate the AC resistance of different conductors' configurations," *Electr. Power Syst. Res.*, vol. 127, 2015.

[24] D. Dai, X. Zhang, and J. Wang, "Calculation of AC Resistance for Stranded Single-Core Power Cable Conductors," *IEEE Trans. Magn.*, vol. 50, no. 11, pp. 1–4, Nov. 2014.

[25] W. T. Weeks, L. L.-H. Wu, M. F. McAllister, and A. Singh, "Resistive and Inductive Skin Effect in Rectangular Conductors," *IBM J. Res. Dev.*, vol. 23, no. 6, pp. 652–660, Nov. 1979.

[26] *WG B2.55 Conductors for the Uprating of Existing Overhead Lines*.

[27] IEEE, "IEEE Std 100-2000 The Authoritative Dictionary of IEEE Standards Terms, Seventh Edition," *IEEE Std 100-2000*. pp. 1–1362, 2000.

[28] T. Asada, W. G. Odendaal, and J. D. van Wyk, "An overview of integratable current sensor technologies," *38th IAS Annu. Meet. Conf. Rec. Ind. Appl. Conf. 2003.*, vol. 2, pp. 1251–1258, 2003.

[29] F. Xie, R. Weiss, and R. Weigel, "Giant-Magnetoresistance-Based Galvanically Isolated Voltage and Current Measurements," *IEEE Trans. Instrum. Meas.*, vol. 64, no. 8, pp. 2048–2054, 2015.

[30] S. D. T. Dewi, C. Panatarani, and I. M. Joni, "Design and development of DC high current sensor using Hall-Effect method," *AIP Conf. Proc.*, vol. 1712, pp. 1–6, 2016.

[31] R. Portas and L. Colombel, "Accuracy of Hall-Effect Current Measurement Transducers in Automotive Battery Management Applications using Current Integration," pp. 1–8, 2007.

[32] Y. W. Kuo, C. L. Li, J. H. Jhang, and S. Lin, "Design of a Wireless Sensor Network-Based IoT Platform for Wide Area and Heterogeneous Applications," *IEEE Sens. J.*, vol. 18, no. 12, pp. 5187–5197, 2018.

[33] W. K. Lee, M. J. W. Schubert, B. Y. Ooi, and S. J. Q. Ho, "Multi-Source Energy Harvesting and Storage for Floating Wireless Sensor Network Nodes with Long Range Communication Capability," *IEEE Trans. Ind. Appl.*, vol. 54, no. 3, pp. 2606–2615, 2018.

Akash Kadechkar was born in Vasai, India. He received the B.E degree in electronics and telecommunication from University of Mumbai, India, in 2012 and M.S. degree in telecommunication, system and networks from Universitat Politecnica de Valencia, in 2016. In 2017, he joined SBI connectors for "SMARTCONNECTOR" project in collabration with Universitat Politècnica de Catalunya where he is currently pursuing his Ph.D. degree in electrical engineering. His research interests include internet of things applied to power transmission and distribution systems for monitoring and control purposes.

Jordi-Roger Riba (M'09) was born in Igualada, Spain, in 1966. He received the M.S. and Ph.D. degrees in physics from the Universitat de Barcelona, in 1990 and 2000, respectively. In 1992, he joined the Universitat Politècnica de Catalunya as an Associate Professor. He is currently with the Motion Control and Industrial Applications Group of the Universitat Politècnica de Catalunya. His current research interests include, high-voltage engineering, modeling and simulation of electromagnetic devices, and electrical machines.

Manuel Moreno-Eguilaz received the M.S. and Ph.D. degrees in industrial engineering from the Universitat Politècnica de Catalunya, Barcelona, Spain, in 1993 and 1997, respectively. He is currently with the Motion Control and Industrial Applications Group and an Associate Professor with the Department of Electronic Engineering, UPC. His current research interests include power electronics, fault tolerant converters, and hybrid electric vehicles.

Josep Sanllehí was born in Manresa, Spain, in 1973. He received the M.S. degree in electrical engineering from the Universitat Politècnica de Catalunya, Barcelona, Spain, in 1997. He joined SBI-Connectors, Barcelona, in 2000, and became the Research and Development Manager in 2012. His current research interests include power transmission and distribution systems, design and simulation of electromagnetic devices, and the internet of things.